Two-Dimensional Crystallography of Amphiphilic Molecules at the Air-Water Interface

Rapid #: -18686639

CROSS REF ID: **5695010770003596**

LENDER: **JNA :: Founders Memorial Library**

BORROWER: **I9W :: Main Library**

TYPE:	Book Chapter
BOOK TITLE:	Neutron and synchrotron radiation for condensed matter studies
USER BOOK TITLE:	Neutron and synchrotron radiation for condensed matter studies
CHAPTER TITLE:	Two-Dimensional Crystallography of Amphiphilic Molecules at the Air-Water Interface
BOOK AUTHOR:	José Baruchel
EDITION:	
VOLUME:	3
PUBLISHER:	
YEAR:	1994
PAGES:	47-68
ISBN:	9783540576938
LCCN:	
OCLC #:	

Processed by RapidX: 2/21/2022 2:50:58 PM

CHAPTER IV

TWO-DIMENSIONAL CRYSTALLOGRAPHY OF AMPHIPHILIC MOLECULES AT THE AIR-WATER INTERFACE

K. KJAER, J. ALS-NIELSEN, M. LAHAV AND L. LEISEROWITZ

IV.1. Introduction

Ever since Langmuir (1917) discovered that amphiphilic molecules, composed of a hydrophobic tail and a hydrophilic head group, form films at the air-water interface, they have elicited wide interest because of their importance in the pure and applied sciences. For example, Langmuir films may be transferred to solid supports for the formation of multilayer Langmuir-Blodgett films (Kuhn et al, 1971), for potential use as piezoelectric sensors (Blinov et al, 1984), soft X-ray monochromators, non-linear optical devices (Girling et al, 1985), and in molecular electronics (Roberts et al, 1978; Morizumu, 1988). Langmuir monolayers serve as useful models for elucidating structure and function of biological membranes in their interactions with lipids, steroids, sugars, proteins and ions (Swalen, 1987). They may also be engineered to induce nucleation of three-dimensional (3-D) crystals from molecules or ions present in the subphase by a form of epitaxial growth (Landau et al, 1985). In this respect they may be used as models for the study of biomineralization in which two-dimensional (2-D) surfaces of biological macromolecules induce the mineralization (Addadi et al, 1987). The design of monolayers with hydrophilic head group arrangements which mimic the surfaces of 3-D crystals also provides a means of examining crystal surface-solvent interactions, for clarifying the effect of the solvent on crystal growth and polymorphism. Furthermore, a knowledge of the characteristics of Langmuir monolayers of water-insoluble amphiphiles should help to throw light on the packing characteristics at the air-water interface of water-soluble amphiphiles, where even less is known about their 2-D arrangements (Weissbuch et al, 1984).

Many of the classical methods used to characterize the properties of Langmuir films do not give direct information on their crystalline packing arrangements. These methods include measurements of surface pressure versus average molecular area, surface potential data (Gaines, 1966), non-linear optics from surfaces (Heinz et al, 1982) and IR spectroscopy (Allara et al, 1985; Gun et al. 1984). Epifluorescence microscopy does furnish some information on crystallinity and morphology on the micron level, but is limited to films containing dye probes (Weiss et al, 1984; Losche et al, 1983). This limitation does not hold for Brewster angle microscopy and is now widely used (Henon and Meunier, 1991; Hönig and Möbius, 1991). Thus, on the molecular level, knowledge of 2-D monolayers had been achieved, in the main, from 3-D crystals. Only recently, with the advent of intense and well collimated X-ray beams of variable wavelength from synchrotron sources, has it became possible to obtain direct structural information on the crystalline properties of these films by X-ray surface diffraction methods.

Here we shall describe X-ray diffraction techniques, which allow one to study films on liquid surfaces *in situ* and review some of the structural results obtained. Emphasis will be placed on monolayer packing arrangements, particularly in terms of the polar head groups. We shall examine crystalline self-aggregation, the effect of pH, ions and solute molecules in the aqueous subphase on molecular packing and crystallinity, and growth and domain size of 2-D crystallites. Finally, we shall discuss the role played by structural complementarity for the induction of 3-D crystal nucleation at the monolayer-solution interface.

For simplicity and ease of presentation we restricted the topics and systems described in the main to our own work. Nevertheless we do wish to cite the pioneering grazing incidence diffraction (GID) studies by other groups. Major contributions were the first GID study of a monolayer of an amphiphile, dipalmitoyl phosphalidylcholine, but on solid support (Seul, Eisenberger, mcConnell, 1983), the detection of a diffraction peak from a phospholipid monolayer on water in a study performed by Möhwald, Kjaer, Als-Nielsen and coworkers (Kjaer et al., 1987) and a GID study of lead-arachidate on water (Dutta et al., 1987). A state of the art review on techniques and properties of organic thin films, including GID results of monolayers on liquid surfaces, has been compiled in a book by Ulman (1991).

IV.2. Surface Sensitive X-ray Methods

The intensity measured in a conventional X-ray scattering experiment is proportional to the irradiated sample volume. This, in turn, is proportional to the penetration depth of the radiation in a sample. For X-rays of about 1 Å wavelength, this penetration ranges from a few micrometers for highly absorbing material to a few millimeters for low absorbing materials. Consequently, the scattering from the surface region is weak compared to that from the bulk. Therefore, a method restricting the penetration depth to the surface region is a

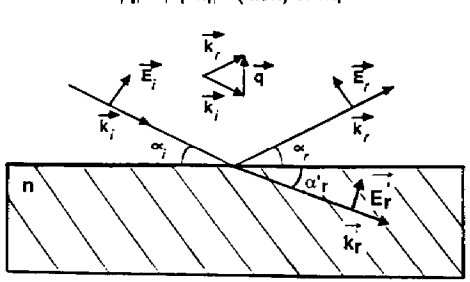

Fig IV.1. — Refracted (E'_r) and reflected (E_r) waves resulting from an incident plane wave with amplitude $|E_i|$ upon an interface between air and a material of refraction index n. Electric fields E are illustrated for one polarization only. The symbol q is the scattering vector, with k_i and k_r the incident and reflected wave vectors of magnitude $2\pi/\lambda$. Note that as $n <_{\sim} 1$, $\alpha'_r < \alpha_i = \alpha_r$. This provides for total reflection at angles $\alpha_r < \alpha_c$, where α_c is the critical angle for total external reflection.

prerequisite for surface diffraction experiments. This restriction can be achieved by using grazing angles of incidence and employing the phenomenon of total external reflection from the surface.

The refractive index n of matter for X-rays in the 1 Å wavelength range is given by (James, 1982):

$$n = 1 - \delta - i\beta \qquad \text{(IV.1)}$$

where $\delta = \rho r_0 \lambda^2/2\pi$, λ is the wavelength, ρ is the electron density and $r_0 = 2.82 \cdot 10^{-13}$ cm is the classical electron radius. Typically δ is of the order of 10^{-5}. The term β is equal to $\eta\lambda/(4\pi)$ where η is the linear absorption coefficient. For X-rays of wavelength $\lambda = 1$Å, absorption is small and $\beta << \delta$.

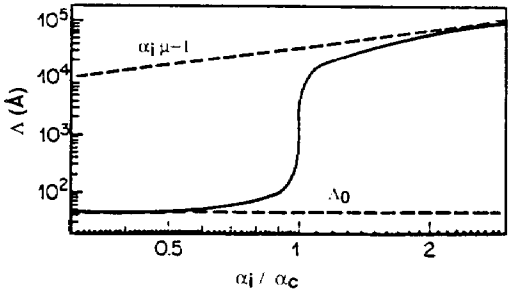

Fig. IV.2. — X-ray beam penetration depth Λ in water at $\lambda = 1.38$ Å versus incidence angle α_i/α_c, where α_c is the critical angle for total external reflection. The limiting value Λ_0 of the penetration depth for $\alpha_i/\alpha_c << 1$ is a characteristic of the material, $= (\pi r_0 \rho)^{-1/2}/4$, independent of the X-ray wavelength λ. For $\alpha_i/\alpha_c >> 1$ the penetration depth is $\alpha_i \mu^{-1}$ where the linear absorption coefficient μ *does* depend on λ.

Consider a plane wave with wavevector $\mathbf{k}_i$ ($k=2\pi/\lambda$) striking at an angle α_i on a planar interface separating a homogeneous medium from the vacuum, as shown in fig. IV.1. The wave will be partially reflected into the vacuum in the direction given by $\alpha_r = \alpha_i$ and partially refracted into the lower medium in the direction given by α'_r. For this case Snell's law yields:

$$n\cos\alpha'_r = \cos\alpha_i \qquad \text{(IV.2)}$$

As $n < 1$, for angles of incidence $\alpha_i \leq \alpha_c = \cos^{-1}(n) = (2\delta)^{1/2}$, the phenomenon of total reflection occurs (Born & Wolf, 1959): the incident wave is totally reflected, while the refracted wave becomes evanescent travelling along the surface. The amplitude of the evanescent wave decays exponentially with depth. The penetration depth of the X-rays in water versus angle of incidence α_i is shown in fig. IV.2. For $\alpha_i < 0.5\ \alpha_c$, the penetration depth is ~50Å. The evanescent wave may therefore be diffracted by crystalline material in a surface layer of that thickness and provide information on its structure. Such diffraction from a surface layer is called grazing incidence diffraction (GID).

In 3-D crystals, diffraction from a set of crystal planes with an interplanar

spacing d occurs only when Bragg's law is obeyed; namely when the scattering vector length $|\mathbf{q}|$ given by $|\mathbf{k}_f - \mathbf{k}_i| = 4\pi\sin\theta/\lambda$ is equal to $2\pi d^*$, where d^* is the reciprocal of d, and the normal to the planes bisects the angle between the incident and outgoing beam. This condition may be expressed mathematically in terms of the reciprocal lattice vectors $\mathbf{d}^* = h\mathbf{a}^* + k\mathbf{b}^* + l\mathbf{c}^*$ where $\mathbf{a}^*, \mathbf{b}^*, \mathbf{c}^*$ are the reciprocal vectors of the unit cell vectors $\mathbf{a}, \mathbf{b}, \mathbf{c}$ and h, k, l are integers that represent the Miller

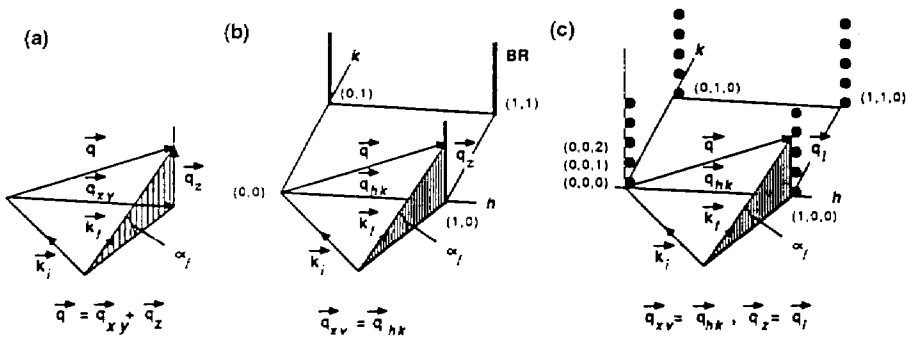

Fig IV.3. — (a) General scattering geometry. $\mathbf{k}_i$ and $\mathbf{k}_f$ are the wavevectors of the incident and diffracted beams respectively. The scattering vector $\mathbf{q} = \mathbf{k}_f - \mathbf{k}_i$ has components $\mathbf{q}_{xy}$ parallel to the monolayer plane and $\mathbf{q}_z$ perpendicular to it. (b) Scattering from a 2-D crystal, depicted in reciprocal space, extends in Bragg rods in the $\mathbf{q}_z$ direction, perpendicular to the plane of the monolayer and of its reciprocal 2-D net. The scattering vector $\mathbf{q}$ must end on an (h,k) Bragg rod for Bragg diffraction to occur. (c) Scattering from a 3-D crystal in a given orientation lies in reciprocal space at the reciprocal lattice points (h,k,l). Diffraction takes place when the scattering vector $\mathbf{q}$ coincides with a specific reciprocal lattice point.

indices of planes with a spacing d_{hkl}. Diffraction only takes place in 3-D crystals when the scattering vector $\mathbf{q}$ coincides with (h,k,l) points of the reciprocal 3-D lattice (Fig. IV. 3c).

For a 2-D crystal, there is no restriction on the scattering vector component $\mathbf{q}_z$ along the film normal; the Bragg scattering extends as continuous rods (BR) through the 2-D reciprocal lattice points (Vineyard, 1982, Feidenhans'l, 1989) (Fig. IV. 3b). The finite thickness of the 2-D crystal causes the BR to extend over finite q_z intervals. The intensity distribution along these intervals is determined by the vertical electron distribution in the molecules and is expressed as the Fourier transform of the resulting electron density along the film normal. This intensity modulation can now be analysed to obtain information, for example, on the molecular packing arrangement in the crystalline part of Langmuir monolayers (Als-Nielsen & Kjaer, 1989, Jacquemain et al, 1989). In addition, detailed information on the electron density distribution in the vertical direction, laterally averaged over both the *ordered* and *disordered* parts of the monolayer can be obtained from the deviation of the measured X-ray reflectivity (Als-Nielsen & Kjaer, 1989) (XR) from the Fresnel law (Born & Wolf, 1959). Finally, grazing incidence X-ray excited fluorescence (Bloch & Eisenberger, 1988)

and X-ray standing wave (Batterman, 1969; Bedzyk et al, 1988, 1990) measurements yield information on the location and concentration of ions bound to the monolayer at the liquid interface. We now discuss the methods of specular X-ray reflectivity (XR) and grazing incidence X-ray diffraction (GID) in some detail.

IV.2.1. Specular Reflectivity (XR)

Specular reflection means that the reflected ray measured is in the plane spanned by $\mathbf{k}_i$ and the vector normal to the surface and that $\alpha_i = \alpha_r$ (Fig. IV. 1). The specular reflectivity of an ideal surface is given by the Fresnel law of optics. In the limit of small angle of incidence, it reduces to:

$$R_F(q_z) = \left| \frac{q_z - [q_z^2 - q_c^2 + i(4\pi\mu/\lambda)]^{1/2}}{q_z + [q_z^2 - q_c^2 + (4\pi\mu/\lambda)]^{1/2}} \right|^2 \qquad \text{(IV.3)}$$

where $q_z = (4\pi/\lambda)\sin\alpha_i$ is the z-component of the vertical scattering vector and $q_c = (4\pi/\lambda)\sin\alpha_c$ is the critical value of q_z for total external reflection. The complex term arises from absorption effects. Neglecting absorption, for $q_z < q_c$, equation (IV.3) yields $R_F = 1$, *i.e.*, total reflection. As q_z is increased beyond q_c, however, R_F decreases and, for $q_z >\sim 4q_c$, approaches $R_F(q_z) \approx (q_c/2q_z)^4$. As the range of interest may extend to $q_z/q_c \approx 30$ or more, reflectivities down to 10^{-8} have to be measured. Hence the importance of high X-ray intensity from a rotating anode generator or a synchrotron source Equation (IV.3) is valid only for an ideally flat surface across which the electron density $\rho(z)$ varies step-like between two constant values. If $\rho(z)$ varies continuously in the surface region, the reflectivity is modified, yielding:

$$R(q_z) = R_F(q_z)\,|\phi(q_z)|^2 \qquad \text{(IV.4)}$$

where

$$\phi(q_z) = (1/\rho_\infty)\int [d\rho(z)/dz]\cdot\exp(iq_z z)dz \qquad \text{(IV.5)}$$

and ρ_∞ is the constant electron density in the subphase bulk. Thus, by measuring $R(q_z)$ it is possible in principle to determine $\rho(z)$, the variation of the electron density normal to the surface, and, in particular, that of a monolayer floating on it. ϕ is a complex function and only its modulus can be derived from the measured reflectivity but not its phase. Thus, one is faced with the usual phase problem of X-ray crystallography. To date virtually all specular reflectivity data have been analysed by fitting a model density $\rho(z)$ to the measured data via equations (IV.3), (IV.4) and (IV.5).

A computationally simple strategy is to represent the monolayer as a stack of slabs (Parrat, 1954), each with a constant density ρ_i and thickness L_i. Two such slabs would be needed for representing, say, a simple fatty acid monolayer. When refining such a *slab* model, a possible choice of fit parameters, then, would be the densities ρ_i and thicknesses L_i of the slabs.

The constant density of the subphase has to be added below the interface. Finally, the model density must be *smeared* out in the z-direction to account for the vertical roughness of the interface. The root-mean-square roughness, σ, is of order 3 Å and stems mainly from thermally excited capillary waves on the water

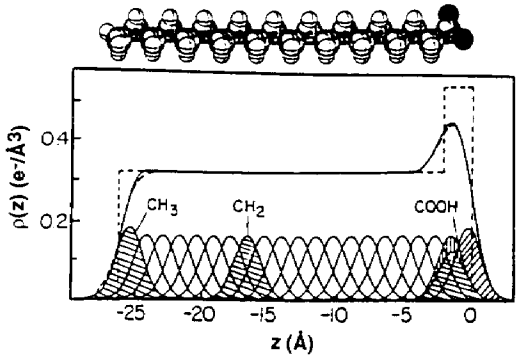

Fig . IV.4. — *Top*. Space filling model of a $C_{19}CO_2H$ molecule.

Bottom. Model electron densities ρ(z). The dashed lines refer to a slab model and a smeared slab model. The full lines refer to an atomic model using CH_3 and CH_2 pseudo-atoms. The contribution of each pseudo-atom (or atom at the CO_2H head group) to the electron density is indicated by Gaussian curves. The two models agree nearly exactly.

surface (Braslau et al, 1988; Als-Nielsen, Kjaer, 1989) It leads to a Debye-Waller factor exp $(-q_z^2\sigma^2)$ in $|\phi(q_z)|^2$ (equation (IV.5)). The rather large value of $\sigma \approx 3$ Å is also the reason that the monolayer may be adequately repesented by the *slab* model. This is illustrated in fig. IV. 4, which shows that the atomic density ρ(z) of a fatty acid monolayer may be represented by a slab model.

IV.2.2. Grazing Incidence Diffraction (GID) and Bragg Rods

In the GID geometry, shown in fig. IV. 5, the angle of incidence α_i of the X-ray beam is kept below the critical angle α_c. This limits the penetration depth of the beam to that of the evanescent wave, so that the background scattering from the subphase is efficiently eliminated. This allows an accurate measurement of the weak diffraction signal originating from the crystalline monolayer. For all the diffraction patterns measured to date, the monolayers were found to be composed of 2-D crystallites randomly oriented on the water surface, namely a 2-D "powder". Hence only a 2θ scan in the monolayer plane is required to measure the diffraction pattern. The analysis is similar to that of a conventional 3-D powder pattern; the reflections can be indexed by two Miller indices, *hk*. Their angular positions $2\theta_{hk}$ corresponding to $q_{hk} = (4\pi/\lambda)\sin\theta_{hk}$ yield the repeat distances $d_{hk} = 2\pi/q_{hk}$ of the 2-D crystal lattice. Their resolution-corrected 2θ-line width (FWHM), Δ, yields the 2-D crystalline coherence length *L* through the Scherrer formula (Guinier, 1968).

$$L = (0.9\lambda)/(\cos\theta_{hk}\Delta) \qquad \text{(IV.6)}$$

The square of the molecular structure factor $|F_{hk}|^2$ integrated along the Bragg rod over the window of q_z seen by the detector, determines the integrated intensity in the peak (James, 1982) . The structure factor F_{hk} is given by:

$$F_{hk}(q_z) = \sum_j f_j \exp i\,(\mathbf{q}_{hk}\cdot \mathbf{r}_j + q_z z_j) \qquad \text{(IV.7)}$$

where f_j is the scattering factor of the atom *j*, $\mathbf{r}_j$ is the vector specifying the (*x*,*y*) position of the atom *j* in the unit cell and z_j is the atomic coordinate along the vertical direction.

More information on the monolayer structure can be obtained by resolving the variation with q_z along the Bragg rod of the intensity $I_{hk}(q_z)$, which is given by:

$$I_{hk}(q_z) = KV(q_z)\,|F_{hk}(q_z)|^2\,DW_{hk}(q_z) \qquad \text{(IV.8)}$$

The observed BR intensity $I_{hk}(q_z)$ is actually a sum over those (*h*,*k*) reflections whose Bragg rods coincide at a particular horizontal 2θ-angle or q_{xy} position. In equation (IV.*8*), the most important variation is due to the molecular structure factor $|F_{hk}(q_z)|$. For chain-like surfactant molecules, the square of the structure factor $|F(q)|^2$ is a bell-shaped function which reaches its maximum when the scattering vector $\mathbf{q} = (q_{hk}, q_z)$ is orthogonal to the molecular axis. Thus, when the molecules are vertical or tilted in a plane perpendicular to q_{hk}, the maximum intensity along the Bragg rod will occur at the horizon, for $q_z = 0$ Å^{-1}. For molecules tilted otherwise, the Bragg rod maximum will occur at a finite q_z, dependent upon both the magnitude and direction of the tilt relative to the in-plane scattering vector $\mathbf{q}_{hk}$. The width of the bell-shaped Bragg rod profile measured in a direction parallel to the molecular axis is inversely proportional to the length of the molecule. This description of F(**q**), may be improved on by calculating F(**q**) according to an atomic model of the molecule as shown by equations (IV.*7*)and (IV.*8*). The exponential (Debye-Waller) factor $DW_{hk}(\mathbf{q}_z) = \exp[-(q^2_{hk}U_{xy} + q^2_z U_z)]$ where U_{xy} and U_z are respectively the mean square displacements in each horizontal direction *x*, *y* and along the vertical direction *z*. They account for the thermal motion of the atoms in the molecule, as well as for ripples on the water surface, which lead to diffuseness of the interface. The factor $V(q_z)$ describes the interference of rays diffracted upwards with rays diffracted down and subsequently reflected back up by the interface (Vineyard, 1982). $V(q_z)$ differs from unity in the vicinity of $q_z = q_c/2$ where it contributes a sharp peak. The factor *K* includes various corrections, such as Lorentz and polarization factors.

There are thus fundamental differences between the BR and XR methods. The BR originate solely from crystalline material and provide information on unit cell dimensions, plane group symmetry, molecular coordinates (indeed at near atomic resolution in favorable cases) and in plane and out-of-plane molecular motion. This is in contrast with XR, which provides information only on the vertical variation of the electron density, averaged over the illuminated area.

An experimental set-up (Fig. IV 6) for the GID geometry (Als-Nielsen et al, 1982) is shown in fig. IV.5. A monochromatic beam is extracted from the incident synchrotron beam by Bragg reflection from a monochromator crystal. By tilting the normal to the reflecting planes out of horizontal plane, the monochromatic beam can be bent down to yield a grazing angle with the liquid surface. Slit S_2, in front of the sample defines a suitable illuminated beam area on the liquid surface. Slit S_3 excludes diffuse scattered background around the reflected beam.

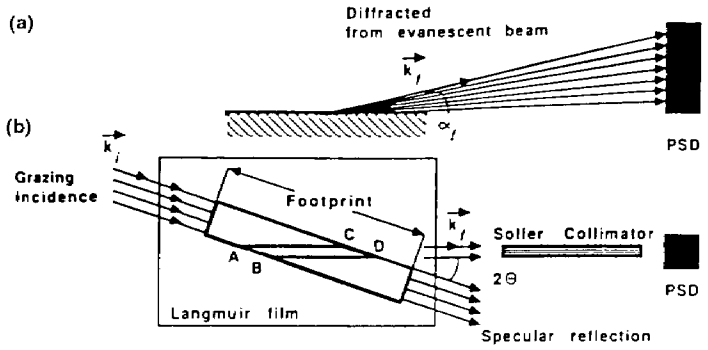

Fig IV.5. — Top and side views of the grazing incidence X-ray diffraction (GID) geometry. The footprint of the grazing incident beam is indicated. The position sensitive detector (PSD) has its axis along the vertical. Only the cross-beam area ABCD contributes to the measured scattering. The Soller collimator consists of thin vertical absorbing foils stacked together to define the horizontal resolution of the detector.

This slit together with a scintillation detector is mounted on an elevator situated on a diffractometer arm which is pivoted around a vertical axis through the sample center. For Bragg rod measurements (Fig. IV. 5), slit S3 is replaced by a Soller collimator giving 1 or 2 mrad collimation and the scintillation counter by a position sensitive detector

IV.3. General Packing Characteristics of Langmuir Monolayers on Water

Before the development of surface X-ray diffraction techniques, molecular arrangements in the three-dimensional state were used to increase understanding of the structure and behaviour of molecules in the monolayer state. Analogous packing is not always possible however, because of environmental differences between the two- and three-dimensional states. Phase diagrams constructed from surface pressure-area (π-A) measurements of Langmuir monolayers revealed phase boundaries, depending upon the pressure, temperature and chain length, but provided little information on their structure. Now, with the recently acquired information from surface-sensitive X-ray techniques, molecular packing within Langmuir films can be determined almost at the atomic level. We will not discuss in any detail Langmuir monolayer structures in terms of their π-A phase diagrams; rather we will focus on their properties in the uncompressed, namely relaxed, state on the solution surface. We will describe examples from different chemical classes studied to date: alcohols, amides, carboxylic acids, salts of the latter, and of α-amino acids (see Table 1 for their chemical formulae and abbreviated names).

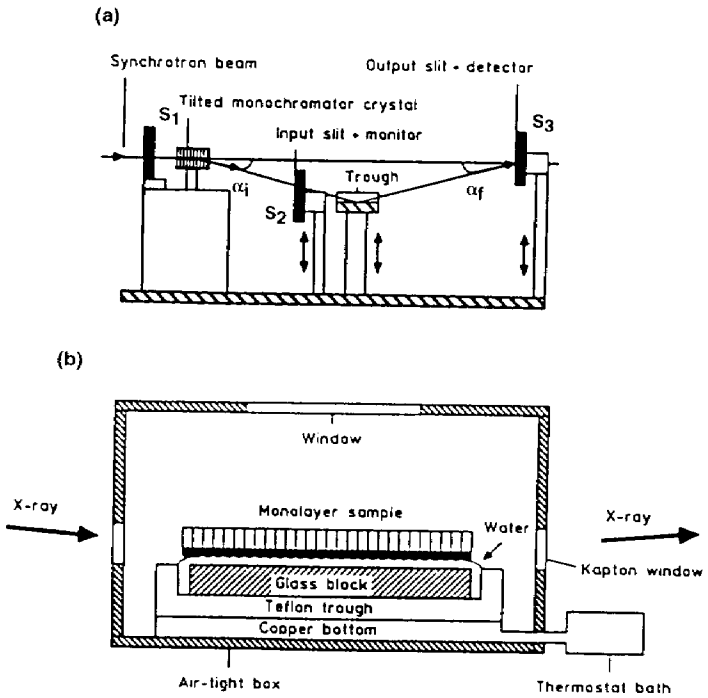

Fig **IV.6.** — Liquid surface diffractometer (beamline D4, X-ray synchrotron source at Hasylab, Hamburg). *a)* Side view of the vertical, scattering plane.

b) Expanded view of the trough showing the monolayer sample spread on a thin film of water. The glass block provides for a thin liquid film (about 0.3 mm thick) to reduce surface capillary waves.

Table 1 : Abbreviations for monolayer compounds discussed

Abbreviation	Full name and chemical formula
C_nOH	Aliphatic primary alcohols $C_nH_{2n+1}OH$
C_nCO_2H	Aliphatic primary acids $C_nH_{2n+1}COOH$
C_nCONH_2	Aliphatic primary amides $C_nH_{2n+1}CONH_2$
PFA	1H,1H,2H,2H-perfluorododecyl-aspartate
	$C_{10}F_{21}C_2H_4OCOCH_2CHNH_3^+CO_2^-$

It is useful at this stage to describe how the unit cell dimensions and molecular orientation may be determined from the GID data for simple cases. We limit the analysis to chain-like molecules with assumed cylindrical symmetry and which pack in three different cells: hexagonal ($a = b$, $\gamma = 120°$), distorted

hexagonal ($a = b$, $\gamma \neq 120°$) which may be more properly described as centered rectangular ($a' = |a+b|$, $b' = |a-b|$), and oblique ($a \neq b \neq |a+b|$). They are shown in fig. IV.7. In a hexagonal cell the molecules are aligned vertically; in the distorted hexagonal cell the molecules are tilted along a symmetry direction and in the oblique cell they are tilted along an arbitrary direction. As mentioned earlier, all Langmuir monolayers studied to date by GID consist of "powders" of randomly ordered 2-D crystallites on the water surface. Thus the GID measurements are not made on single crystals so that the diffraction spectra consist of coinciding Bragg rods of reflections (h,k,q_z) and $(\bar{h}, \bar{k},q_z)$; the notation $\{h,k,q_z\}$ designating both reflections. In general, the intensity distribution along their two coinciding

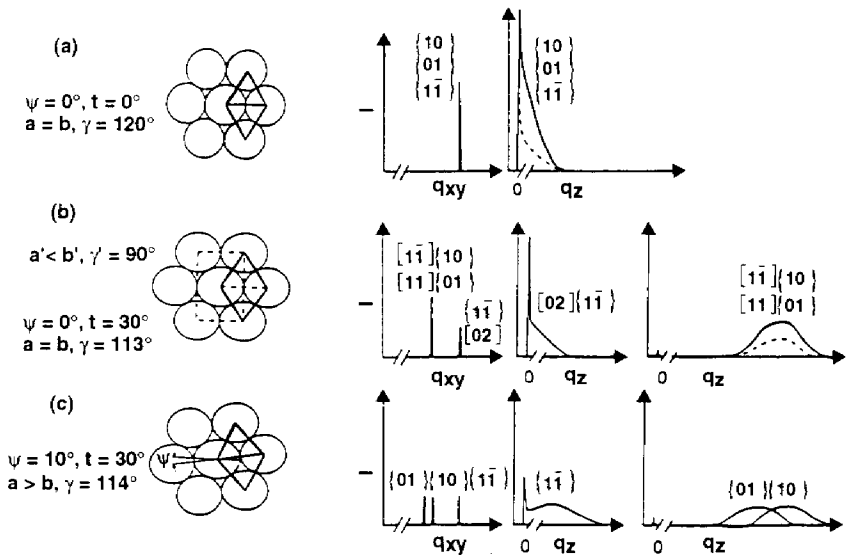

Fig IV.7. — Three structures and diffraction from a monolayer of close-packed cylindrical chains. The left colum shows schematic top views of molecular packing in hexagonal, distorted hexagonal and oblique unit cells. The second column shows the q_{xy}-pattern integrated over the vertical scattering vector component q_z. Last two columns show the Bragg rods integrated over the corresponding q_{xy}. When more than one reflection coincide, the dashed lines represent the intensity from individual reflections as indicated by the $\{h, k\}$ indices. The solid line represents the intensity from a 2-D powder sample; that is the sum of the intensities indicated by dashed lines. When the molecular axis is perpendicular to the water surface the lattice is hexagonal (a), and the $\{1,0\}$,$\{0,1\}$ and $\{1,\bar{1}\}$ reflections are equivalent. The Bragg rod obtained from the single in-plane diffraction peak has its maximum at $q_z = 0$ Å^{-1}. When the molecular axis is tilted towards nearest neighbors (b), the hexagonal cell is distorted to a centered rectangular cell (rectangular notation at top, distorted hexagonal notation at bottom). The degeneracy of the three reflections is partially lifted resulting in two peaks. The Bragg rod of the two equivalent reflections $\{1,0\}$ and $\{0,1\}$($[1,1]$, $\{1,\bar{1}\}$ in the rectangular notation) is centered at $q_z \geq 0$ Å^{-1}, the position of the center depending upon the extent of molecular tilt. The Bragg rod of the $\{1,\bar{1}\}$ reflection is still centered at $q_z = 0$ Å^{-1}. Finally, a tilt of the molecular axis in a non-symmetry direction, yields an oblique 2-D cell (c). The degeneracy is completely lifted and the peak positions of the three Bragg rods determine the tilt angle as well as the azimuthal angle ψ.

Bragg rods will be different unless the monolayer structure has a twofold symmetry along the vertical axis.

The hexagonal cell has three equivalent lattice spacings d_{hk}: d_{10}, d_{01} and $d_{1,\bar{1}}$ The GID spectrum from these three reflections will appear as a single peak with all corresponding Bragg rods peaking at $q_z = 0$ Å^{-1} (Fig. IV. 7a). The corresponding GID pattern for the distorted hexagonal cell will comprise two peaks; one a doublet arising from the coinciding $\{1,0\}$ and $\{0,1\}$ reflections, and the remaining $\{1,\bar{1}\}$ peak (Fig. IV 7b). The separation between the two peaks depends upon the deviation of the angle γ from 120°. In the oblique cell the extent to which the three peaks $\{1,0\}$, $\{0,1\}$ and $\{1,\bar{1}\}$ are resolved (Fig. IV. 7c), depends upon the deviation from centered rectangular cell symmetry.

Thus the 2-D crystal lattice parameters (a, b, γ) can be extracted, from the horizontal position of the maxima of the Bragg peaks. Precise information on the molecular orientation can be easily extracted from the BR data assuming the aliphatic chains are uniformly and rigidly tiled in the monolayer (Als-Nielsen & Kjaer, 1989; Jacquemain et al, 1989, 1990). The angle t between the molecular axis and the surface normal is given by:

$$\cos\psi_{hk} \cdot \tan t = q_z^0 / |q_{hk}| \qquad \text{(IV.9)}$$

where q_z is the position of the maximum along the Bragg rod and ψ_{hk} is the azimuthal angle between the molecular tilt direction projected onto the xy plane and the reciprocal lattice vector q_{hk}. The molecules will therefore be perpendicular to the surface when, for all reflections (h,k), q_z tends to 0 Å^{-1}.

IV.4. Crystalline Self-Assembly of Non-compressed Monolayers

GID has proven a powerful tool for the detection of crystallite self-aggregates formed by insoluble amphiphilic molecules and for the determination of their size and structure, almost at the atomic level. Indeed GID has demonstrated that this crystalline self-assembly is a widespread phenomenon for fluorocarbon (Jacquemain et al, 1990; Barton et al, 1992) and hydrocarbon amphiphiles (Jacquemain et al, 1991; Leveiller et al, 1991). We will focus on hydrocarbon systems, although the fluorocarbons exhibit a greater extent of crystallinity, presumably because of a higher stiffness of their carbon backbone and a more favorable van der Waals interaction between their chains (Jacquemain et al, 1992).

IV.4.1. Structure determination of self-assembled crystallites

Experiments have shown that lowering the temperature considerably enhances the tendency for crystalline self-aggregation of hydrocarbon chain monolayers. Thus GID studies were performed at low temperature on several monolayers C_n-X with different head groups X, i.e. C_nOH, (n=16, 20,23, 30, 31), $C_{19}OCOC_nOH$ (n=9,10), $C_{29}CO_2H$, $C_{19}CONH_2$, $C_{29}CONH_2$ and $C_{19}CONHC_2H_4CO_2H$. The probable packing characteristics of the spontaneously formed crystallites could be extracted from the GID data (Jacquemain, et al 1991; Weissbuch et al, 1992; Leveiller, et al 1992; Wang et al, 1992), as well as making use of atom-atom potential energy calculations to reduce ambiguities . We present here a brief description of the deduced packing arrangements of the acid

(X = CO_2H) the alcohol (X = OH), and the amide (X = $CONH_2$) monolayer.

The GID pattern for the monolayer of $C_{29}CO_2H$ in the uncompressed state at +5°C (Fig. IV.8) comprises two low-order reflections which indicates a rectangular cell (Table 2) for which the symmetry-related {1,1} and $\{1,\bar{1}\}$ reflections coincide and the {0,2} reflection is separate and distinct. The intensity profile of the Bragg rod for the {0,2} reflection has its maximum at $q_z = 0 Å^{-1}$; hence the molecular axis lies in a plane perpendicular to the long *b* axis of the unit cell. The angle of tilt of the hydrocarbon chain within this plane can be extracted from the intensity profile of the {1,1} and $\{1,\bar{1}\}$ Bragg rod making use of eqn. (9). The chain is tilted at 27° towards nearest neighbors along the short *a* axis. This angle is compatible with the length of 5.53 Å. These two lengths yield a molecular tilt angle of 26°(=arcos 4.94/5.53) in the uncompressed state, in the close agreement with the value derived from the Bragg rod profile.

In order to establish the cell symmetry and molecular packing, we now divert to review layered 3-D crystal structures of long chain acids and alcohols (Small, 1986). In each layer the molecules are related by a glide so that neighbouring hydrocarbon chains have parallel mean axes, but are in a mutually perpendicular orientation when viewed down the mean axis; the motif is described as orthogonal $O_\perp$ (Small, 1986). Common to all these structures is a rectangular subcell, which is a projection of the unit cell onto a plane perpendicular to the molecular axis and dimensions a_p = 5.0 Å, b_p = 7.4 Å, corresponding to a cross-sectional area of 18.5 $Å^2$. The calculated 2-D cells of the monolayers projected onto a plane perpendicular to the molecular axis perfectly match the rectangular subcell of the 3-D crystal structures. Thus it was deduced that the $C_{29}CO_2H$ acid monolayer molecules appear in the orthogonal $O_\perp$ packing, *i.e.*, they are related by a glide along the *a* axis in a primitive rectangular cell in plane group symmetry *p*11*g* as shown in figure IV. 9. (The symbol *p* specifies a primitive unit cell and *g* a glide plane perpendicular to the *b* axis, so naturally the glide is parallel to the *a* axis. Note that for plane group *p*1*g*1 , the glide would be perpendicular to the *a* axis and so parallel to *b*).

An *ab initio* demonstration of the orthogonal $O_\perp$ packing of the chains of $C_{29}CO_2H$ in plane group *p*11*g* was provided by an analysis of the BR data making use of eqns. (7) and (8), and a reliability index R_w,* complemented by lattice energy calculation. The molecular arrangement was varied, about its deduced position by rotation about three Eulerian angles and by molecular translation along the *y* axis. The model in which the molecular chain axes are centered parallel between the glide planes, tilted at an angle of 26° and oriented so as to form the orthogonal $O_\perp$ packing gave the lowest R_w index. Although the calculated Bragg rod profiles compared well with the observed ones (Fig. IV. 9), it was not possible to distinguish between two structures which differed only in rotation by 180° about the molecular axis. This ambiguity was eliminated, and the correctness of the model structure established through lattice energy calculations.

*The weighted reliability index R_w is defined by $\sum_i \omega_o^{1/2}|I_o - I_c| / \sum_i \omega_o^{1/2} I_o$. The summation is over all the *i* individual Bragg rod points, where I_o is the observed intensity of the i^{th} point, ω, the square root of its weight = $1/\sigma(I_o)$, and I_c, the intensity calculated from the structure factor formula (Eqn. 7) making use of the atomic *xyz* coordinates of the molecular. R_w is analogous to the reliability index used for 3-D crystal structure refinement.

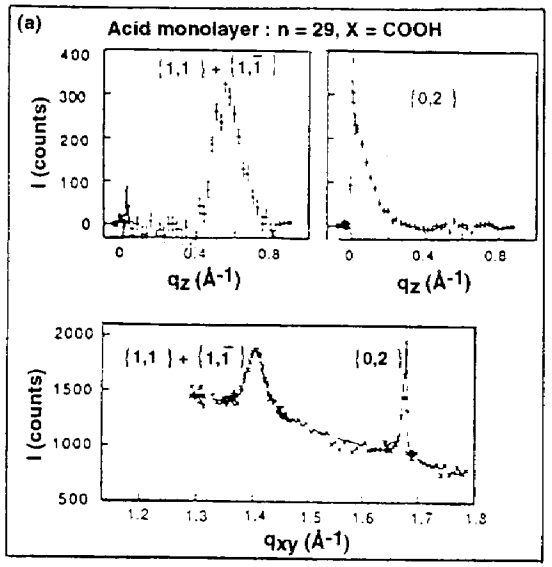

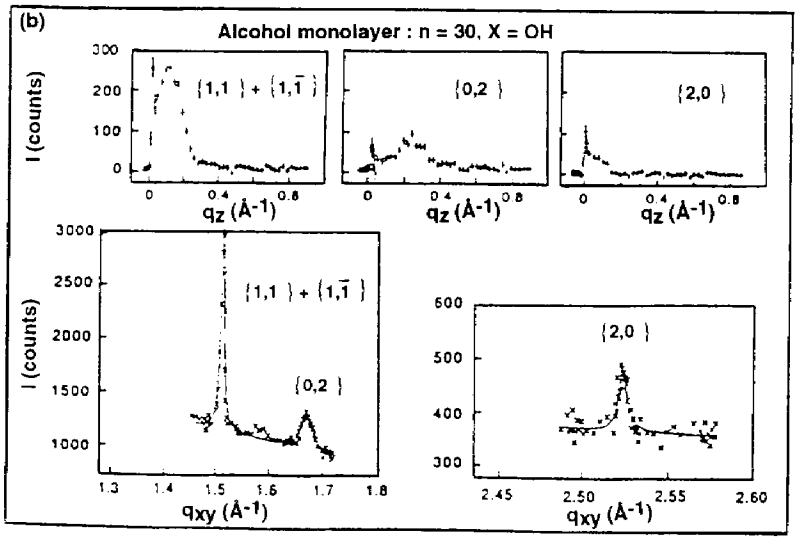

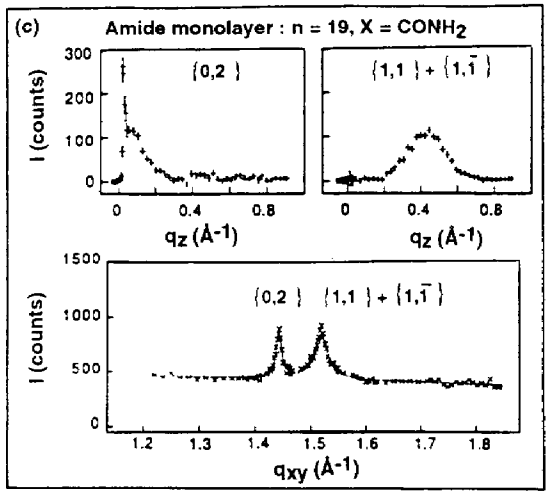

Fig. IV.8. — GID spectra of monolayers at zero surface pressure and at 5°C over pure water. *Top.* q_z resolved Bragg rod profiles. *Bottom*: q_z integrated Bragg peaks. The $\{h, k\}$ reflection assignment is indicated on the two data sets: (a) $C_{29}CO_2H$; (b) $C_{30}OH$; (c) $C_{19}CONH_2$.

The Bragg rod data of uncompressed monolayers of alcohols $C_{30}OH$ and $C_{31}OH$ were analyzed (Wang et al, 1993) in a manner similar to that adopted for $C_{29}CO_2H$. The molecules crystallize in a rectangular cell (Table 2) in space group $p1g1$ in the orthogonal $O_\perp$ motif (Fig. IV. 9). Unlike the $C_{29}CO_2H$ structure, the alcohol molecular chains are tilted at a low angle of ~ 10° and in the direction of the long b axis. In these systems the presence of the {2,0} reflection enabled a reliable determination of the molecular mean squared motion U_{xy} parallel to the water surface. yielding a value of ~ 0.08Å^2, in keeping with the molecular motion found in layers of 3-D crystal structures containing hydrocarbon chains.

The proposed packing arrangement of the 2-D crystal structure of $C_{19}CONH_2$ (Fig. IV. 9) was based on the GID data and 3-D crystal strucures of long chain diamides. (Jacquemain, 1991). The molecular chains of C_{19} $CONH_2$ are stacked

Table 2. Bragg Peak Analysis of the Different Monolayers $C_nH_{2n+1}X$[a]

compound n, x	d_{11} and $d_{1\bar{1}}$ (*L*)	d_{02} (*L*)	d_{20} (*L*)	*a*	*b*
30, OH	4.15 (≥1000)	3.75 (23)	2.49 (>1000)	4.99	7.49
29, CO_2H	4.44 (150)	3.72 (>1000)	5.53	7.44	
19, $CONH_2$	4.34 (200)	4.12 (550)	4.69	8.69	

[a]For each h, k reflection the d- spacing (in Å) is given and the crystal correlation length L (Å). The unit cell axes a, b (Å) are for a rectangular cell.

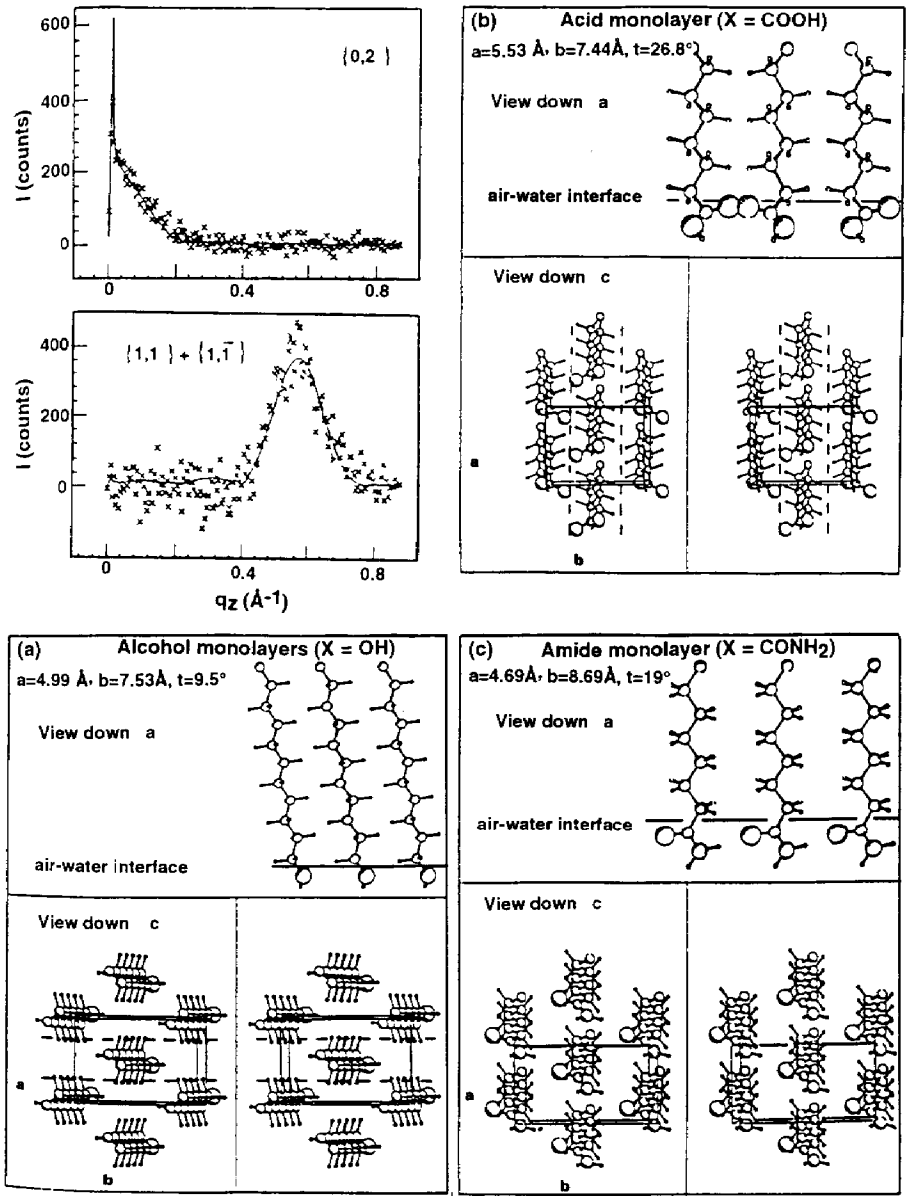

Fig. IV.9. — Side and top (stereoscopic) view of the packing arrangements. Only the head group and maximally 11 CH_2 groups of each molecule are shown. Glide symmetry elements, are shown as dashed lines. *(Top)* Observed and calculated (full line) Bragg rods and packing arrangement of the $C_{29}CO_2H$ acid monolayer. *(Bottom)* Packing arrangements of the $C_{30}OH$ and $C_{19}CONH_2$ monolayers

into rows by translation along the 4.7Å *a* axis with the molecular axis tilted at an angle of 18° to the vertical. These molecules are interlinked by N-H...O hydrogen bonds by translation symmetry along the diagonal (**a**+ **b**)/2.

IV.4.2. Correlation between crystalline self-assembly and calculated lattice energies

Positional correlation lengths of crystallites of monolayers such as $C_{29}CO_2H$, $C_{19}OCOC_nOH$ (n=9,10) and C_nOH (n=16,20) where the molecules exhibit a pronounced tilt in the range 20-30° are very anisotropic (e.g. see Table 2 for the $C_{29}CO_2H$ monolayer); these lengths are decidedly shorter in the direction parallel to the molecular tilt than perpendicular to it. Lattice energy calculations were used also to help throw light on coherence length anisotropy. The idea implemented involved calculation of the attachment energy of different (h,k) lines. Such energy computations performed on $C_{29}CO_2H$ and $C_{19}OCOC_nOH$ n=9,10 (Leveiller et al, 1992), showed that the attachment energy was found to be weaker for the molecular row corresponding to the broad {1,1} reflection than to the sharp {0,2} reflection, as exemplified in Fig. IV. 9 and Table 2 for $C_{29}CO_2$.

These results are a corollary of the observation that the stronger the interactions between the amphiphilic molecules on the liquid surface, the more crystalline the material in the self-aggregated state (Jacquemain et al, 1992b, Leveiller et al, 1992). This observation was shown to hold for the fatty acids C_nCO_2H ($_n$=13,19,21,29) over pure water; the longer the chain the more crystalline the material. This increased crystallinity with chain length in the acids may be correlated with the contribution to the lattice energy of ~2Kcal/mole per CH_2 group in the chain. This simple correlation is in keeping with the observation, alluded to earlier, that fluorocarbon amphiphiles are more crystalline than their hydrocarbon counterparts because of more favorable interchain van der Waals interactions.

IV.5. Influence of Ions and Solutes on Monolayer Organization

IV.5.1. Solute Binding and Growth and Dissolution of Monolayers

The binding of solute molecules to hydrophilic groups of monolayers allows us to probe not only its effect on the growth, stability and dissolution of 2-D crystals, but to simulate interactions between the surface of a 3-D crystal and solvent or solute molecules. It has been observed that addition of solute species in the subphase can deter crystalline self-aggregation of monolayers or can bring about dissolution of the crystallites, processes which can be monitored as a function of time (Jacquemain et al, 1990, 1992a).

IV.5.2. Ion Binding from Solution

The interfacial region between a charged surface and an electrolyte is central to many processes such as those occurring during electrodeposition, ion transport through biological membranes, preparation of LB films (Kuhn & Mohius, 1971) biomineralization (Addadi et al, 1987) and induced oriented nucleation of inorganic 3-D crystals under Langmuir monolayers (Landau et al 1986; 1989; Mann et al, 1988). X-ray reflectivity measurements, demonstrated that metal ions, when present in solution, interact closely with the charged monolayer head groups at the interface (Kjaer et al, 1989; Richardson et al, 1987; Daillant et al, 1989). However, the question was still open as to whether the ion distribution near such charged ordered surfaces is crystalline.

A weak indication of lateral ionic order is provided by GID data of uncompressed PFA monolayers spread over highly basic KOH subphases (pH = 11.5). According to an analysis of the GID data, the K^+ ions occupy ordered sites bridging oxygen atoms of neighbouring PFA molecules (Jacquemain et al, 1990).

An unambiguous demonstration of ordered binding of counterions, with a lateral coherence length of ~ 1000Å was provided by uncompressed cadmium arachidate monolayers over a subphase with an adjusted pH of 8.8 using ammonia as a base, at temperatures lower than 9°C (Leveiller et al, 1991). The diffraction spectrum showed ten distinct peaks (Fig. IV. 10a) , seven of which

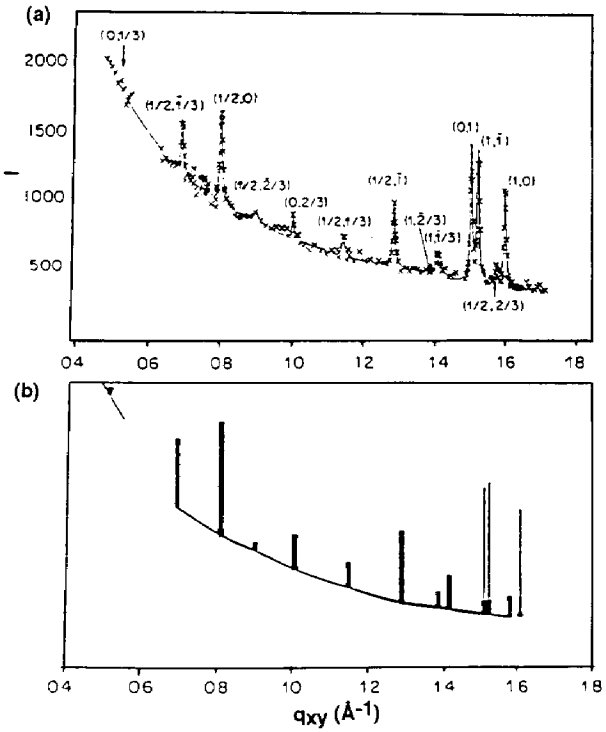

Fig. IV.10 — Arachidic acid monolayer ($C_{19}CO_2H$) over a 10^{-3} M $CdCl_2$ subphase (pH = 8.8) in the uncompressed state and at low temperature (9° C).

(a) GID peaks and reflections assignment. The reflections with integer indices correspond to the scattering arising from the arachidate moieties. The reflections with fractional indices correspond to the scattering from a 2-D layer of $CdOH^+$ ions. (b) Calculated powder pattern for the cadmium net, superimposed on background scattering. The three peaks labeled with thin lines are the arachidate "triplet".

were attributed to the cadmium layer. The remaining three peaks were deduced to stem primarily from the arachidate layer, on the basis of their Bragg rod profiles and q_{xy} positions and so denoted as the arachidate "triplet". The diffraction peaks of the cadmium lattice whose BR profiles were flat and extended, indicative of a thin monoatomic layer, could be indexed according to a 2x3 supercell of the arachidate cell. The packing arrangement of the arachidate molecules could be established from a fit to BR profiles of the arachidate triplet (Leveiller et al, 1993). Specular X-ray reflectivity measurements have shown that the molar ratio of cadmium to arachidate is 5:6 or 1:1, so that the counter layer must consist essentially of CdOH+ ions. The refined Cd positions in the 2 x 3 supercell, containing either 5 or 6 cadmium atoms, gave a very good fit (Fig. IV. 10b) to the observed seven diffraction peaks arising from the counterionic layer.

IV.6. Crystallization of Molecules under Monolayers with a Similar Head Group.

Langmuir monolayers have been shown to induce oriented crystallization from solution of protein(Uzgiris and Kornberg, 1983) and other organic and inorganic compounds (Landau et al, 1985; Mann et al 1988, Weissbuch et al, 1990; Heywood et al, 1991; Gavish et al, 1990). These studies were motivated by their revelance to crystal nucleation, to two-dimensional ordering at the water surface of amphiphilic molecules and to biomineralization. Mechanisms for the oriented crystallization include structural fits and electrostatic attractions. Structures of some monolayers were determined by GID to establish the epitaxial relation, e.g. that of an α-amino acid surfactant (Grayer Wolf et al, 1987) which induces crystallization of glycine (Landau et al, 1985). Here we describe induced nucleation of ice by alcohol monolayers, which involves a structural fit, as shown by GID.

IV.6.1. Nucleation of Ice by Monolayers

Pure water can be supercooled to temperatures as low as -40° C. Therefore the induction or inhibition of the nucleation of ice, in particular through the role of auxiliaries such as membranes or proteins, has far-reaching ramifications for both the living and non-living world.

Here we review experiments conducted in order to design two-dimensional surfaces which raise the ice nucleation temperature (Gavish et al, 1990; Popovitz-Biro et al, 1993). These experiments involved the freezing of drops of water covered with monolayers of aliphatic alcohols (C_nX, X = OH). The structure of hexagonal ice may be described for the oxygen atoms in terms of layers parallel to the *ab* plane where $a = b = 4.5$ Å, $\gamma = 120°$ For purpose of comparison we may describe this *ab* net in terms of a *c* - centered rectangular net $a' = |a + b| = 4.5$Å and $b' = |a - b| = 7.8$Å. Advantage was taken of the observation already discussed in section 4.1 that the uncompressed monolayers of $C_{30}OH$ and $C_{31}OH$ over water at 5°C are crystalline and pack in a rectangular net $a = 5.0$Å, $b = 7.5$Å (Jacquemain et al 1991; Wang et al, 1993) which is similar in dimension to the $a'b'$ rectangular representation of hexagonal ice at 0° C. We may, to a first approximation, regard the alcohol 2-D structures of $C_{30}OH$, and $C_{31}OH$ as *c* - centered, according to Fig. IV. 9 for $C_{30}OH$. The uncompressed monolayer of the

carboxylic acid $C_{29}CO_2H$ has axial dimensions $a = 5.5$ Å, b=7.4 Å (Table 2), and so exhibits a large lattice mismatch to ice. Thus a structural similarity can be proposed for the OH head groups of the alcohol monolayer and the *ab* layer structure of ice, but no such similarity exists for the corresponding carboxyl head groups of the fatty acid monolayer (see Fig. IV. 9).

The results of the ice nucleation temperature ("freezing point") measurements (Fig.IV. 11) show that aliphatic chain alcohols are more efficient ice nucleators than the corresponding carboxylic acids (Gavish et al, 1990). The freezing temperature depends not only on chain length but also on chain parity (*i.e.*, *n* odd or even) of the alcohol $C_nH_{2n+1}OH$ (Fig. IV. 11). This trend suggests that, at the temperature of ice nucleation, the orientation of the alcohol OH groups in the odd and even analogues are not the same. Studies attempting to elucidate these questions are underway.

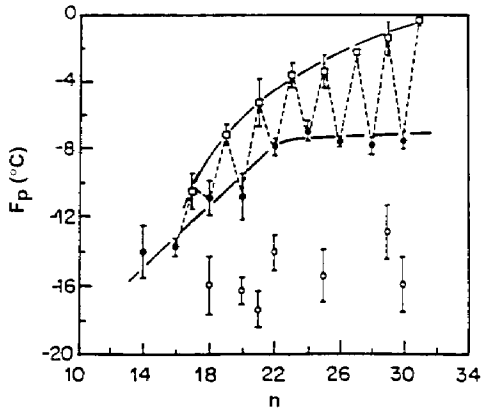

Fig. IV.11 — Freezing points (Fp) of drops of supercooled water covered by monolayers of alcohols C_nOH (*n* even • and *n* odd ◦) and carboxylic acids C_nCO_2H (o). Freezing point curves are drawn separately for alcohols with *n* odd and *n* even.

REFERENCES

ADDADI L. , MORADIAN J. , SHAY E., MAROUDAS N.G., WEINER S. , 1987- Proc. Natl. Acad. Sci. U.S.A. 84 , 2732.

ALLARA D.L. , NUZZO R.G. , 1985 - Langmuir 1, 52.

ALS-NIELSEN J. , CHRISTENSEN F., PERSHAN P.S., 1982 - Phys. Rev. Lett. 48, 1107.

ALS-NIELSEN J., PERSHAN P. , 1983 - Nucl. Instrum. Meth. 208, 545.

ALS-NIELSEN J. , in S. Ebashi, E. Rubenstein and M. Koch (Eds.): Handbook of Synchrotron Radiation Vol. III, North Holland Amsterdam, in press.

ALS-NIELSEN J. , KJAER K. in T. Riste and D. Sherrington (Eds.): 1989 -The Proceedings of the NATO Advanced Study Institute, Phase Transitions in Soft Condensed Matter, Series B Vol. 211, Plenum Press New York p. 113.

ALS-NIELSEN, J. , MOHWALD H. in S. Ebashi, E. Rubenstein and M. Koch (Eds.): Handbook of Synchrotron Radiation Vol IV , North Holland Amsterdam, in press.

BARTON S.W. , GOUDOT A., BOULOUSSA O., RONDELEZ F., LIN B., NOVAK F., ACERO A., RICE S.A., 1992 - J. Chem. Phys. 96, 1343.

BATTERMAN B.W. , 1964 - Phys. Rev. 133, 1759; BATTERMAN B.W., 1969, Phys. Rev. Letts. 22, 703.

BEDZYK M.J. , BILDERBACK D.H., BOMMARITO G.M., CAFFREY M., SCHILDKRAUT J.S. 1988 - Science 241, 1788; BEDZYK M.J. , BOMMARITO G.M. , CAFFREY M. , PENNER T.L. , 1990 - Science 248, 52.

BERGE B. , FAUCHEUX L. , SCHWAB K. , LIBSHABER A. , 1991 - Nature 350, 322.

BLINOV L.M. , DUBININ N.V. , MIKHNEV L.V. , YUDIN S.G. , 1984- Thin Solid Films 120, 161;

BLOCH J.M. , EISENBERGER P. , 1988 - Nucl. Instrum. Meth. B31, 468; BLOCH J.M. , 1988 -Phys. Rev. Lett. 61, 2941.

BORN, M. , WOLF E. , 1959 - Principles of Optics, MacMillan, New York.

BRASLAU A. , PERSHAN P.S., SWISLOW G. , OCKO B.M. , ALS-NIELSEN J. , 1988 - Phys. Rev. A 38, 2457.

DAILLANT J. , BOSIO L. , BENATTAR J.J., MEUNIER J. , 1989 - Europhys. Lett. 8, 453.

DUTTA, P., PENG, J.B., LIN, B., KETTERSON, J.B., PRAKASH, M., 1987 - Phys. Rev. Lett. 58, 2228.

FEIDENHANS'L R., 1989 - Surf. Sci. Rep. 10, 105.

GAINES G.,1966 - Insoluble monolayers at the Liquid-Gas Interface, Interscience, New York .

GAVISH M. , POPOVITZ-BIRO R. , LAHAV, M. , LEISEROWITZ L. , 1990 - Science 250, 973.

GIRLING I.R. , KOLINSKY P.V. , CADE N.A. , EARLS J.D. , PETERSON I.R. , 1985- Optics Commun. 55, 289.

GRAYER WOLF S. , LEISEROWITZ L. , LAHAV M. , DEUTSCH M. , KJAER K. , ALS-NIELSEN J. , 1987 - Nature 328, 63.

GUINIER A. , 1968 - X-Ray Diffraction, Freeman San Francisco ch. 5.1.

GUN J. , ISCOVICI R. , SAGIV J 1984 - J. Colloid Interface Sci. 101, 201.

HEINZ T.F. , CHEN C.K. , RICARD D. , SHEN Y.R. , 1982 - Phys. Rev. Lett. 48, 478.

HENON, S., MEUNIER, J., 1991 - Rev. Sci. Instrum. 62, 936.

HÖNIG, D., MÖBIUS, D., 1991 - J. Phys. Chem. 95, 4590.

HEYWOOD B.R. , RAJAM S. , MANN S. , 1991- J. Chem. Soc. Faraday Trans. 87, 735.

JACQUEMAIN D. , GRAYER WOLF S., LEVEILLER , F. , LAHAV M. , LEISEROWITZ L. , DEUTSCH M. , KJAER K. , ALS-NIELSEN J., 1989 - Coll. de Phys. 50, C7 p.29.

JACQUEMAIN D. , GRAYER WOLF S. , LEVEILLER F., LAHAV M., LEISEROWITZ L. , DEUTSCH M. , KJAER K., ALS-NIELSEN J., 1990- J. Am. Chem. Soc. 112, 7724.

JACQUEMAIN D. , LEVEILLER F. , WEINBACH S.P. , LAHAV M., LEISEROWITZ L. , KJAER K. , ALS-NIELSEN J. , 1991- J.Am.Chem.Soc. 113, 7684.

JACQUEMAIN D., GRAYER WOLF S., LEVEILLER F., DEUTSCH M., KJAER K., ALS-NIELSEN J., LAHAV M., LEISEROWITZ L., 1992A - Angew. Chem. 31, 130.

JACQUEMAIN D., GRAYER WOLF S., LEVEILLER F., FROLOW F., EISENSTEIN M., LAHAV M., LEISEROWITZ L. 1992B - J. Am. Chem. Soc. 114, 9983.

JAMES R.W. , 1982 -The Optical Principles of the Diffraction of X-Rays, Ox Bow, Woodbridge CT.

KJAER, K., ALS-NIELSEN, J., HELM, C.A., LAXHUBER, L.A., MÖHWALD, H., 1987 - Phys. Rev. Lett. 58, 2224.

KJAER K. , ALS-NIELSEN J., HELM C.A., TIPPMAN-KRAYER P., MOHWALD H. , 1989 -J. Phys. Chem. 93 , 3200.

KUHN H. , MOBIUS D., 1971- Angew. Chem. 83, 672.

LANDAU E.M. , GRAYER WOLF S., SAGIV J. , DEUTSCH M., KJAER K. , ALS-NIELSEN J. , LEISEROWITZ L., LAHAV M., 1989- Pure & Appl. Chem. 61, 673.

LANDAU E.M., POPOVITZ-BIRO R., LEVANON M. , LEISEROWITZ L., LAHAV M. , 1986- Mol. Cryst. Liq. Cryst. 134, 323.

LANDAU E.M., LEVANON, M. , LEISEROWITZ, L., LAHAV M., SAGIV J. 1985- Nature 318, 353; LANDAU E.M., GRAYER WOLF, S., LEVANON, M. , LEISEROWITZ L., LAHAV M. , SAGIV J. , 1989-J. Am. Chem. Soc. 111 , 1436.

LANGMUIR I., 1917 - J. Am. Chem. Soc. 39 , 1848.

LEVEILLER F. , JACQUEMAIN D. , LAHAV M. , LEISEROWITZ L. , DEUTSCH M. , KJAER K. , ALS-NIELSEN J. , 1991 - Science 252, 1532.

LEVEILLER F. , JACQUEMAIN D., LEISEROWITZ L., KJAER K., ALS-NIELSEN J., 1992 - J. Phys. Chem. 96, 10380.

LEVEILLER F., BOHM C., JACQUEMAIN F., MOHWALD D.H., LEISEROWITZ L., KJAER K., ALS-NIELSEN J. Submitted for publication 1993.

LOSCHE M. , SACHMANN E. , MOHWALD H., 1983 - Ber Bunsenges. Phys. Chem. 87, 848.

MANN S., HEYWOOD B.R. , RAJAM S. , BIRCHALL J.D. , 1988- Nature 334, 692,

MORIZUMI T. , 1988 - Thin Solid Films 160, 413.

PARRAT L.G. 1954 - Phys. Rev. 95, 359.

POPOVITZ-BIRO R., WANG J.L., MAJEWSKI J., LEISEROWITZ L., LAHAV M., 1993. Submitted for publication

RICHARDSON R.M. , ROSER S.J. , 1987 - Liquid crystals 2, 797. RICHARDSON Grundy, R.M. , ROSER S.J. , PENFOLD J. , WARD R.C. , 1988 - Thin Solid Films 159, 43.

ROBERTS G.G. , PAUDE K.P. , BARLOW W.A. , 1978 - Proc. Inst. Electr. Eng. Part I, 125, 169.

SEUL, M., EISENBERG, P., McCONNELL, H.M., 1983 - Proc. Natl. Acad. Sci. U.S.A. 80, 5795.

SMALL D.M. , 1986 - The Physical Chemistry of Lipids, Handbook of Lipid Research Vol.4, Plenum Press.

SWALEN J.D. , ALLARA D.L. , ANDRADE J.D., CHANDROSS, E.A. GARROF S. , ISRAELACHVILI, J., McCARTHY, T.J. , MUNRAY R. PEASE, R.F., RABOLT, J.F. , WYNNE, K.J. , YU H. , 1987- Langmuir 3, 932.

ULMAN, A. In Introduction to Ultrathin Organic Films. Academic Press, N.Y. 1991.

UZGIRIS E.E. , KORNBERG R.D. , 1983 - Nature 301, 125.

VINEYARD G. , 1982 - Phys. Rev. B 26, 4146. FEIDENHANS R. , 1989, Surf. Sci. Rep. 10, 105.

WANG J.L., JACQUEMAIN, D., LEVEILLER F., KJAER K., ALS-NIELSEN J., LAHAV M., LEISEROWITZ L., 1993 - Submitted for publication.

WEIS R.M., McCONNELL, H.M., 1984 - Nature 310, 47.

WEISSBUCH I., BERKOVIC G., LAHAV M., LEISEROWITZ L., 1990 - J. Am. Chem. Soc. 112, 5874.

WEISSBUCH I., et al., to be published 1993.